

# Deduction of an invariant-mass spectrum $M(\Sigma\pi)$ for $\Lambda(1405)$ with mixed $T_{\Sigma\pi \leftarrow K^-p}$ and $T_{\Sigma\pi \leftarrow \Sigma\pi}$ from Hemingway's data on the $\Sigma^+(1660) \rightarrow \Lambda(1405) + \pi^+ \rightarrow (\Sigma\pi)_{I=0} + \pi^+$ processes

Maryam Hassanvand,<sup>1,2</sup> Yoshinori Akaishi,<sup>1,3</sup> and Toshimitsu Yamazaki<sup>1,4</sup><sup>1</sup>*RIKEN, Nishina Center, Wako, Saitama 351-0198, Japan*<sup>2</sup>*Department of Physics, Isfahan University of Technology, Isfahan 84156-83111, Iran*<sup>3</sup>*College of Science and Technology, Nihon University, Funabashi, Chiba 274-8501, Japan*<sup>4</sup>*Department of Physics, University of Tokyo, Bunkyo-ku, Tokyo 113-0033, Japan*

(Received 28 February 2015; revised manuscript received 1 June 2015; published 9 October 2015)

We formulated the  $\Lambda(1405)$  (abbreviated as  $\Lambda^*$ )  $\rightarrow (\Sigma\pi)^0$  invariant-mass spectra produced in the  $K^- + p \rightarrow \Sigma^+(1660) + \pi^-$ , followed by  $\Sigma^+(1660) \rightarrow \Lambda(1405) + \pi^+ \rightarrow \Sigma\pi + \pi^+$ , processes at  $p(K^-) = 4.2$  GeV/c, in which both the incident channel for a quasibound  $K^-p$  state and its decay process to  $(\Sigma\pi)^0$  were taken into account realistically. We calculated  $M(\Sigma\pi)$  spectral shapes using mixed transition matrices,  $T_{21} = T_{\Sigma\pi \leftarrow K^-p}$  and  $T_{22} = T_{\Sigma\pi \leftarrow \Sigma\pi}$ , for various theoretical models involving  $\Lambda^*$ . The asymmetric spectra were compared to old experimental data of Hemingway, and it was found that the mixing of the two channels, written as  $(1-f)T_{21} + fT_{22}$ , gave a better result than considering the individual channels, yielding  $f = 0.376_{-0.019}^{+0.021}$ ,  $M(\Lambda^*) = 1406.6_{-3.3}^{+3.4}$  MeV/c<sup>2</sup> and  $\Gamma = 70 \pm 2$  MeV, nearly consistent with the 2014 PDG values.

DOI: [10.1103/PhysRevC.92.045202](https://doi.org/10.1103/PhysRevC.92.045202)

PACS number(s): 21.45.-v, 13.75.-n, 21.30.Fe, 21.90.+f

## I. INTRODUCTION

Historically, in 1959 Dalitz and Tuan [1] predicted the existence of a strange quasibound state of  $K^- + p \rightarrow \Sigma + \pi$  with  $I = 0$  in their analysis of experimental  $\bar{K}N$  scattering data. In 1961 its experimental evidence was found from the mass spectrum,  $M[(\Sigma\pi)^0]$ , in the reaction  $K^- + p \rightarrow (\Sigma\pi)^0 + \pi^+\pi^-$  at  $p_{K^-} = 1.15$  GeV/c [2]. The resonant state of  $\Lambda(1405)$  with  $J = 1/2, I = 0, S = -1$ , called  $\Lambda(1405)$ , is located below the  $\bar{K}N$  threshold, and decays to  $\Sigma\pi$ . After half a century, this state has been certified as a four-star state in Particle Data Group data [3]. According to Dalitz and Deloff [4], from an  $M$ -matrix fit to experimental data of Hemingway [5], the mass and width of this resonance were obtained to be  $M = 1406.5 \pm 4.0$  MeV/c<sup>2</sup> and  $\Gamma = 50 \pm 2$  MeV. It is interpreted as a quasibound state of  $\bar{K}N$  coupled with continuum state of  $\Sigma\pi$ . The 27-MeV binding energy of  $K^- + p$  indicates a strongly attractive  $\bar{K}N$  interaction, and a series of deep and dense  $\bar{K}$  nuclear systems were predicted based on the  $K^-p$ - $\Sigma\pi$  coupled-channel calculations [6–11]. In the mean time, chiral dynamics theories suggested two poles [12,13] in the coupled  $\bar{K}N - \Sigma\pi$  scheme, to which counter arguments were given [14]. In the double-pole hypothesis the  $\bar{K}N$  attraction mainly arises from the upper pole lying around 1420 MeV/c<sup>2</sup> or higher, and thus becomes much weaker, and may thus contribute only to shallow  $\bar{K}$  bound states. The question as to whether the  $K^-p$  bound state is deep or shallow is of great importance from the viewpoints of kaon condensation [15,16], but still remains controversial. Experiments of Braun *et al.* at CERN [17] and of Zychor *et al.* at COSY [18] provided some interesting data, but they are statistically poor. More recently, Esmaili *et al.* [19,20] analyzed old bubble-chamber data of stopped- $K^-$  on  ${}^4\text{He}$  [21] with a resonant capture process, and found the best-fit value to be  $M = 1405.5_{-1.0}^{+1.4}$ . Hassanvand *et al.* [22] analyzed recent data of HADES on  $p + p \rightarrow p + K^+ + \Lambda(1405)$  [23], and subsequently deduced  $M = 1405_{-9}^{+11}$  MeV/c<sup>2</sup> and  $\Gamma = 62 \pm 10$  MeV. Now, the new PDG values [24] have been revised

to be  $M = 1405.1_{-1.0}^{+1.3}$  and  $\Gamma = 50.5 \pm 2.0$ , upon adopting the consequences of these analyses. Concerning the most basic  $\bar{K}$  bound state,  $K^-pp$  predicted in [7,11], experimental evidence for deeply bound states has been obtained by FINUDA [25], DISTO [26], and J-PARC E27 [27].

In the present paper we provide a theoretical formulation to analyze the old experimental data of Hemingway at CERN in the reaction  $K^-p \rightarrow \Sigma^+(1660) + \pi^- \rightarrow \Lambda(1405) + \pi^+ + \pi^- \rightarrow (\Sigma\pi)_{I=0} + \pi^+ + \pi^-$  processes at 4.2 GeV/c. The intermediate resonance state  $\Sigma^+(1660)$  was well selected in the initial reaction channel of  $K^- + p \rightarrow \Sigma^+(1660) + \pi^-$ . These data have been analyzed by many theoreticians, but ended with unsatisfactory consequences. One of the reasons might be because they did not examine the nature of the transitions from  $\Sigma^+(1660)$  in terms of *both*  $K^- + p \rightarrow \Sigma + \pi$  (expressed by  $T_{21} = T_{\Sigma\pi \leftarrow K^-p}$ ) and  $\Sigma + \pi \rightarrow \Sigma + \pi$  (expressed by  $T_{22} = T_{\Sigma\pi \leftarrow \Sigma\pi}$ ). There were uncertainties in the selection between  $T_{21}$  and  $T_{22}$ , and the data were often fitted by only  $T_{22}$ . Also, fitting was made for a Breit-Wigner shape, which is not justified because the resonance zone exceeds the kinematically allowed limits [22,28].

We show in Fig. 1 the level scheme of the decay of  $\Sigma^+(1660)$  into a  $K^-p$  quasibound state embedded in the continuum of  $(\Sigma + \pi)_{I=0}$ . There are two possible diagrams (a) and (b), which correspond to  $T_{21}$  and  $T_{22}$ , respectively. Regarding the formation process, it is not obvious which of  $T_{21}$  or  $T_{22}$  is responsible for the Hemingway process that undergoes through  $\Sigma^+(1660)$ . We thus set up arbitrarily mixed transition matrices,  $T_{21} + T_{22}$ , for any kind of the  $\bar{K}N$  interaction model so as to find the best fit with the experimental data without any prejudice. In addition, it is vitally important to take care of the broad distribution of the  $\Lambda(1405)$  resonance, whose mass ranges between  $M(\Sigma) + M(\pi) = 1330$  MeV/c<sup>2</sup> and  $M(K^-) + M(p) = 1430$  MeV/c<sup>2</sup>. Under these conditions the resonance shape can never be of a symmetric Breit-Wigner type, but should be very much skewed. Here, we follow our former treatments [22].

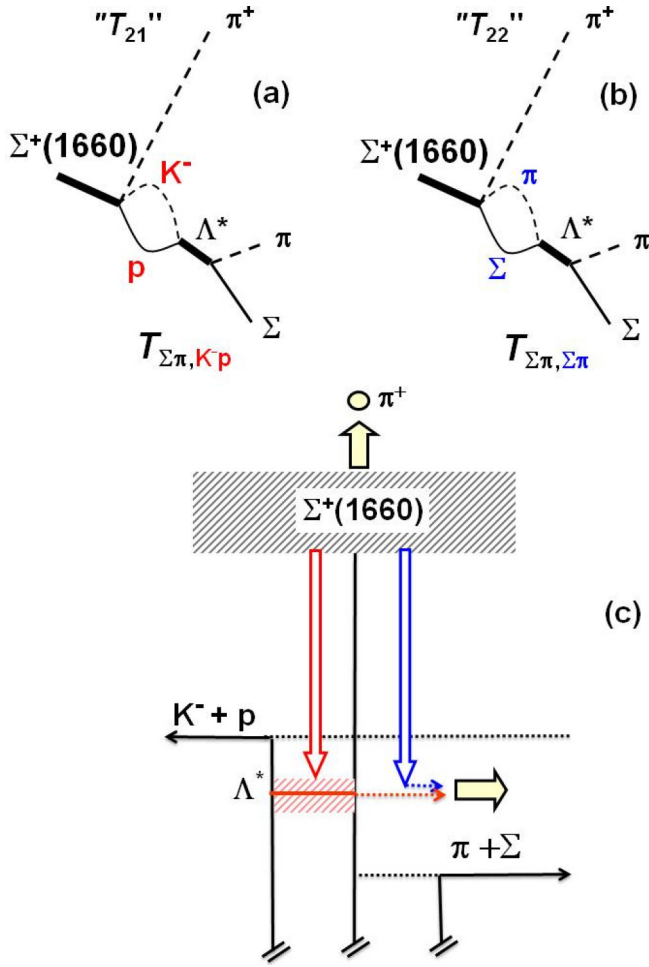


FIG. 1. (Color online) Diagrams for the  $\Sigma^+(1660) \rightarrow \pi^+ + \Lambda^* \rightarrow \pi^+ + (\Sigma\pi)^0$  reaction for (a) the process through  $T_{\Sigma\pi \leftarrow K^-p}$  ( $T_{21}$ ) and (b) the process through  $T_{\Sigma\pi \leftarrow \Sigma\pi}$  ( $T_{22}$ ) channels. (c) Schematic picture of the coupled-channel model in which the  $K^-p$  quasibound state is treated as a Feshbach resonance, including two channels,  $\bar{K}N$  and  $\Sigma\pi$ .

## II. FORMULATION

A coupled-channel treatment of  $\Lambda(1405)$  employed in this paper is described in [22,28]. We use a set of separable potential with a Yukawa-type form factor,

$$\langle \vec{k}'_i | v_{ij} | \vec{k}_j \rangle = g(\vec{k}'_i) U_{ij} g(\vec{k}_j), \quad (1)$$

$$g(\vec{k}) = \frac{\Lambda^2}{\Lambda^2 + \vec{k}^2}, \quad \Lambda = \frac{m_B c}{h}, \quad (2)$$

with  $\Lambda$  being a range parameter, depending on the mass of exchanged boson ( $m_B$ ), and

$$U_{ij} = \frac{1}{\pi^2} \frac{\hbar^2}{2\sqrt{\mu_i \mu_j}} \frac{1}{\Lambda} s_{ij}, \quad (3)$$

where  $i(j)$  stands for the  $\bar{K}N$  channel, 1, or the  $\Sigma\pi$  channel, 2, and  $\mu_i$  ( $\mu_j$ ) is the reduced mass of channel  $i(j)$ , and  $s_{ij}$ 's are nondimensional strength parameters. We obtain  $s_{11}$  and  $s_{12}$  from the  $M$  and  $\Gamma$  values of an arbitrarily chosen  $K^-p$  state

to be used to calculate the  $\Sigma\pi$  invariant masses. It means that, in our model, the strength parameters depend on the binding energy and the width of  $\Lambda(1405)$  state as explained in detail in Ref. [28]. In our coupled-channel model presented here, it is obvious that the properly determined two parameters,  $s_{11}$  and  $s_{12}$ , for any value of  $s_{22}$ , can represent the resonance pole without loss of generality. Here, we adopt  $s_{22} = -0.7$ , which gives  $U_{22}/U_{11} = 4/3$  for  $\Lambda(1405)$  as in a ‘‘chiral’’ model, and  $\Lambda = 3.9 \text{ fm}^{-1}$ .

As described in Ref. [19] in detail, we treat the  $K^-p$  quasibound state as a Feshbach resonance, and the coupled-channel transition matrix,

$$\langle \vec{k}'_i | t_{ij} | \vec{k}_j \rangle = g(\vec{k}'_i) T_{ij} g(\vec{k}_j), \quad (4)$$

satisfies the following matrix equation:

$$T_{ij} = U_{ij} + \sum_{i=1} U_{il} G_l T_{lj}, \quad (5)$$

with a loop function  $G_l$ :

$$G_l = \frac{2\mu_l}{\hbar^2} \int d\vec{q} g(\vec{q}) \frac{1}{k_l^2 - q^2 + i\epsilon_0} g(\vec{q}). \quad (6)$$

The solution is given in a matrix form by

$$T = [1 - UG]^{-1}U \quad (7)$$

with

$$(UG)_{lj} = -s_{lj} \sqrt{\frac{\mu_j}{\mu_l}} \frac{\Lambda^2}{(\Lambda - ik_j)^2}, \quad (8)$$

and  $k_j$  is a relative momentum in channel  $j$ .

The transition matrix elements in this framework are  $T_{11}$ ,  $T_{12}$ ,  $T_{21}$ , and  $T_{22}$ , which constitute the experimentally observable quantities below the  $\bar{K} + N$  threshold,  $(-1/\pi)\text{Im}(T_{11})$ ,  $|T_{21}|^2 k_2$  and  $|T_{22}|^2 k_2$ , where  $k_2$  is the  $\Sigma\pi$  relative momentum. The first term corresponds to the  $\bar{K}N$  missing-mass spectrum and is proportional to the imaginary part of the scattering amplitude given in Fig. 15 of Hyodo-Weise [13]. The second term with  $g^2(k_2)g^2(k_1)$  is a  $\Sigma\pi$  invariant mass from the conversion process,  $\bar{K}N \rightarrow \Sigma\pi$  (called in this paper as ‘‘ $T_{21}$  invariant mass’’) which coincides with the  $\bar{K}N$  missing-mass spectrum in the mass region below the  $\bar{K} + N$  threshold through the following formula, as has been derived from an optical relation [19]:

$$\text{Im}T_{11} = |T_{21}|^2 \text{Im}(G_2). \quad (9)$$

Therefore the observation of a  $T_{21}$  invariant-mass spectrum is just the observation of the imaginary part of the scattering amplitude given in [13]. The third term with  $g^4(k_2)$  is a  $\Sigma\pi$  invariant-mass spectrum from the scattering process,  $\Sigma\pi \rightarrow \Sigma\pi$  (called in this paper as ‘‘ $T_{22}$  invariant mass’’). Two observables of  $\bar{K}N - \Sigma\pi$  coupled channels [as mentioned above  $T_{11}$  channel is associated with  $T_{21}$  by Eq. (9)] calculated by Hyodo and Weise’s chiral two-channel model [13] and also in the framework of  $\Lambda(1405)$  ansatz of Akaishi and Yamazaki [6] represented in Fig. 1 (upper) of Esmaili’s paper [20]. This figure shows that the two curves of the chiral model have peaks at different positions (1420 and 1405 MeV/ $c^2$ ) but Akaishi and Yamazaki’s  $T_{21}$  and  $T_{22}$

invariant mass spectra have peaks near  $1405 \text{ MeV}/c^2$ . Within this theory the peak positions can be varied. The main purpose of this paper is to determine the peak position of these two channels by comparing with experimental observables.

The level scheme for  $\Sigma^+(1660) \rightarrow \Lambda^* + \pi^+ \rightarrow (\Sigma\pi)^0 + \pi^+$  is shown in Fig. 1. It proceeds to either the  $K^- + p$  channel forming the  $\Lambda^*$  resonance, then decaying to  $\Sigma\pi$ , which corresponds to the diagram (a) ( $T_{21}$ ). Another process is to emit  $\Sigma + \pi$ , which forms  $\Lambda^*$ , then decaying to  $\Sigma + \pi$ , as represented by  $T_{22}$  in (b). Therefore there are two ‘‘incident channels’’ to bring  $\Lambda(1405)$  state: one is  $K^- + p$  and the other is  $\Sigma + \pi$ . This picture was also shown by Geng and Oset [29] in a different framework. In the mechanism given in the present paper, the resonance state  $\Lambda^*$  is a Feshbach state, in which a quasibound  $K^- p$  state is embedded in the continuum of  $\Sigma\pi$ .

The theoretical framework for calculating the decay rate of  $\Lambda(1405)$  to  $(\Sigma\pi)^0$  was given in detail in [14,28]. To calculate the decay rate function, we take into account the emitted  $\Sigma$  and  $\pi$  particles realistically, following the generalized optical formalism in Feshbach theory [30]. The decay function,  $G(x)$  with  $x = M_{\Sigma\pi}$  being the invariant mass, is not simply a Lorentzian but is skewed because the kinetic freedom of the decay particles is limited. The general form of  $G(x)$  is given as

$$G(x) = \frac{2(2\pi)^5}{(\hbar c)^2} \frac{E_\Sigma E_\pi}{E_\Sigma + E_\pi} \text{Re}[k | \langle k | t | k_0 \rangle|^2], \quad (10)$$

where  $k_0$  and  $k$  are the relative momenta in the initial and final states written as

$$\vec{k}_0 = \frac{c\sqrt{\lambda(x, m_K, M_p)}}{2\hbar x} \quad (11)$$

and

$$\vec{k} = \frac{c\sqrt{\lambda(x, m_\pi, M_\Sigma)}}{2\hbar x} \quad (12)$$

with

$$\lambda(x, m_1, m_2) = (x + m_1 + m_2)(x + m_1 - m_2) \\ \times (x - m_1 + m_2)(x - m_1 - m_2). \quad (13)$$

The kinematical variables in the c.m. framework of the decay process of  $T_{21}$  and  $T_{22}$  channels are given in Fig. 2 of Ref. [22].

In this way the decay rate of  $\Lambda(1405) \rightarrow \Sigma + \pi$  process via two so-called ‘‘incident channels’’  $K^- + p \rightarrow \Lambda(1405)$  and  $\Sigma + \pi \rightarrow \Lambda(1405)$  as shown in Fig. 1(a) and (b) is obtained. Equation (10) with Eqs. (1) and (2) is completed and the invariant mass spectra of  $T_{21}$  and  $T_{22}$  channels calculated using Eq. (4). As we show in Fig. 3(c) in our previous work [22], these spectra do not depend on the incident energy of the Hemingway experiment,  $E(K^-) = 4.2 \text{ GeV}$ , in the laboratory and for all values of  $E(K^-)$  the shape of the spectrum does not change.  $G(x)$  is a unique function of  $x = M_{\Sigma\pi}$  (invariant mass) associated with  $m_i$  (mass of  $K^-$ ,  $p$ ,  $\Sigma$ , and  $\pi$  particles) and is bounded by the lower end ( $M_l = M_\Sigma + M_\pi = 1328 \text{ MeV}/c^2$ ) and the upper end ( $M_u = M_p + M_{K^-} = 1432 \text{ MeV}/c^2$ ).

It should be noted here that by changing the width of the spectrum, the position of the peak in  $G(x)$  moves, and is

different from the position of the pole ( $M = 1405 \text{ MeV}/c^2$ ). In the next section we present the  $G(x)$  function as  $S(x; M, \Gamma)$  to obtain the  $\chi^2$  value.  $S(x; M, \Gamma)$  spectrum has a peak and a width in the region of the experimental data ( $1330\text{--}1430 \text{ MeV}/c^2$ ). We first consider the binding energy and the width of the pole as two free parameters and calculate the spectrum. Then we compare these theoretical curves to the experimental data using a  $\chi^2$  test which gives us the degree of fitting as to how well our model actually reflects the data. In Sec. III we discuss some results of current model and compare them to Hemingway’s experimental data.

### III. FITTING RESULTS

The 11 points of Hemingway’s data, ( $N_i \pm \sigma_i$ ) for  $i = 1, \dots, n$ , cover a mass spread from  $M = 1330 \text{ MeV}/c^2$  ( $\Sigma\pi$  threshold) to  $M = 1430 \text{ MeV}/c^2$  ( $K^- p$  threshold) [5]. Previously, these data were fitted by a Breit-Wigner function,  $K$ -matrix calculation, and another model, namely, an extended cloudy bag model, as given in Ref. [5]. The Breit-Wigner function makes a poor fit to the data, yielding a mass and width of  $\Lambda(1405)$  as  $1391 \pm 1 \text{ MeV}/c^2$  and  $32 \pm 1 \text{ MeV}$ , while the  $K$ -matrix method results in  $1411.4 \pm 2.0 \text{ MeV}/c^2$  and  $79.6 \text{ MeV}$  for its mass and width [4].

The main purpose of the present paper is to fit the experimental data to our theoretical curves given in the preceding section so that the best fit with the least  $\chi^2$  value can be deduced. The theoretical spectral curve,  $S(x; M, \Gamma)$ , is a function of the invariant-mass ( $x = M_{\Sigma\pi}$ ) with the mass ( $M$ ) and the width ( $\Gamma$ ) of the  $\Lambda^*$  resonance as parameters. Then,  $\chi^2$  will be defined as

$$\chi^2(M, \Gamma) = \sum \left( \frac{N_i - S(x_i; M, \Gamma)}{\sigma_i} \right)^2, \quad (14)$$

where  $N_i$  are the experimental data,  $\sigma_i$  are the errors of the data.

Using the  $\chi^2$  method, the best possible fit has been obtained between the spectrum shape of the  $\Sigma\pi$  invariant mass, given from the  $T_{21}$  ( $K^- p \rightarrow \Sigma\pi$ ) and  $T_{22}$  ( $\Sigma\pi \rightarrow \Sigma\pi$ ) channels and Hemingway’s experimental data. For this work we faced a two-dimensional plane consisting of the mass of  $\Lambda^*$  ( $M$ ) and its width ( $\Gamma$ ), so that by varying each of these parameters  $\chi^2$  values could be obtained. Our purpose in this section is to describe how we obtained a pair of ( $M_{\Lambda^*}, \Gamma$ ) that give the minimum  $\chi^2$ .

We first overview how the theoretical  $S(M, \Gamma)$  curves behave in comparison with the experimental data in Fig. 2, where calculated curves are shown together with the experimental data. The upper (or lower) two frames, specified with (a) [or (c)] and (b) [or (d)] in the figure, give curves for the  $T_{21}$  (or  $T_{22}$ ) channel with assumed masses of  $M = 1405 \text{ MeV}/c^2$  (left) and  $1420 \text{ MeV}/c^2$  (right), both with five different curves corresponding to assumed values of  $\Gamma = 30, 40, 50, 60,$  and  $70 \text{ MeV}$ . The experimental data reveal a broad bump at around  $1400\text{--}1420 \text{ MeV}/c^2$  with a long lower tail. A very characteristic feature of the theoretical curves is their asymmetric and skewed shapes, which can be understood in terms of the broad resonance located in the limited mass range. When  $\Gamma$  is small, the curve shows a distinct peak at around the assumed mass,  $M$ , but the lower tail part cannot be accounted

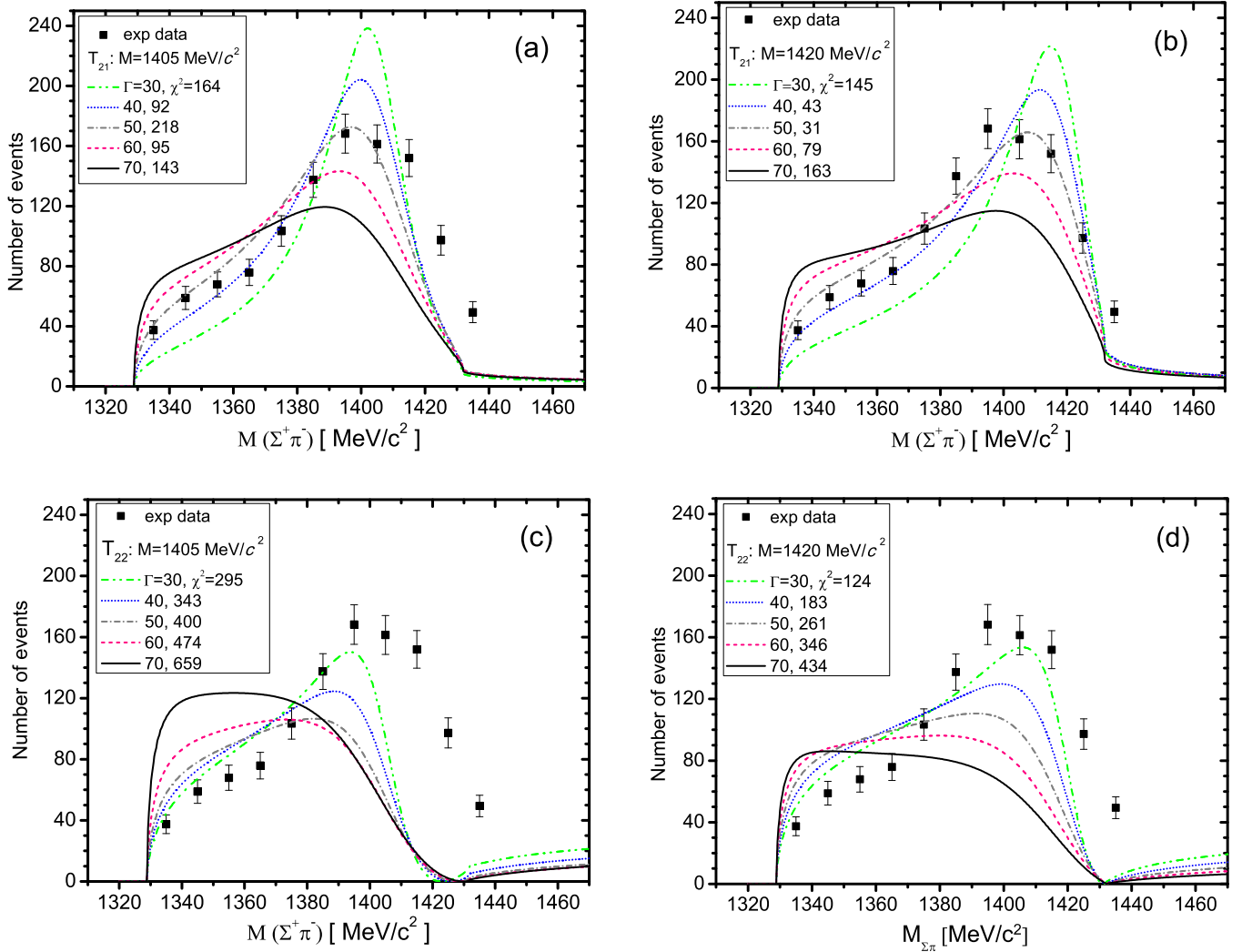


FIG. 2. (Color online) Spectra of the  $|T_{21}|$  channel [(a),(b)] and the  $|T_{22}|$  channel [(c),(d)] for a fixed  $M_{\Lambda^*}$  of 1405 [(a),(c)] and 1420 [(b),(d)]  $\text{MeV}/c^2$  and for  $\Gamma$  values from 30 to 70  $\text{MeV}$  by 10  $\text{MeV}$  steps. The experimental values of Hemingway [5] are shown by closed circles with error bars. The  $\chi^2$  values from fitting to each curve are shown.

for. On the other hand, when  $\Gamma$  becomes large, the lower tail component increases too much. At around  $\Gamma \sim 50$   $\text{MeV}$  a very crude agreement is attained, but the  $\chi^2$  value is still large at around 50 compared with the expected  $\chi^2$  value of  $n_{\text{DF}} = n - 3 \approx 8$ .

Figure 2 shows typical  $T_{21}$  and  $T_{22}$  spectra with two assumed masses,  $M = 1405$  and  $1420$   $\text{MeV}/c^2$ . The very broad character of the curves does not seem to allow good agreement with the experimental data at all. These figures show  $\bar{K}N$  threshold effects on the  $\Sigma\pi$  invariant mass spectrum,  $|t_{21}|^2 k_2$  and  $|t_{22}|^2 k_2$ . When the width is sufficiently narrow, the spectrum is almost symmetric with a peak close to the assumed pole position [22]. When the width becomes wide, the peak position is lowered from the pole position, and spectrum shape changes to a skewed one; this is the  $\bar{K}N$  threshold effect on the spectrum. Although the  $M$  value is assumed to be constant, the peak position shifts upon changing the  $\Gamma$  value. In the case of a fixed  $\Gamma$ , as we change the  $M$  value, the peak position shifts slightly from the pole position (compare the right frame of Fig. 2 to the left one).

Because of the poor agreements between the experiment and theory using  $T_{21}$  and  $T_{22}$  alone, one might give up any fitting, but we now attempt to consider the case of mixed  $T_{21}$  and  $T_{22}$  transitions. This means that the shape of the spectrum is not produced from the  $T_{21}$  or  $T_{22}$  channel alone, but a mixture of both channels with different contributions is considered as follows:

$$T_{\text{mixed}} = (1 - f) T_{21} + f T_{22} \quad (15)$$

with  $f$  being a complex constant parameter. The percentages of  $T_{21}$  and  $T_{22}$  are  $|1 - f|^2 / (|1 - f|^2 + |f|^2)$  and  $|f|^2 / (|1 - f|^2 + |f|^2)$ , respectively.

For this purpose, various combinations of the two channels were taken into account, and the shape of the spectra was plotted again. The situation is very complicated, since the vector addition of the complex functions  $T_{21}$  and  $T_{22}$  behaves in very strange ways. We show all the fitted curves with smoothly varying parameter values in the Appendix of a preprint version of this paper [31].

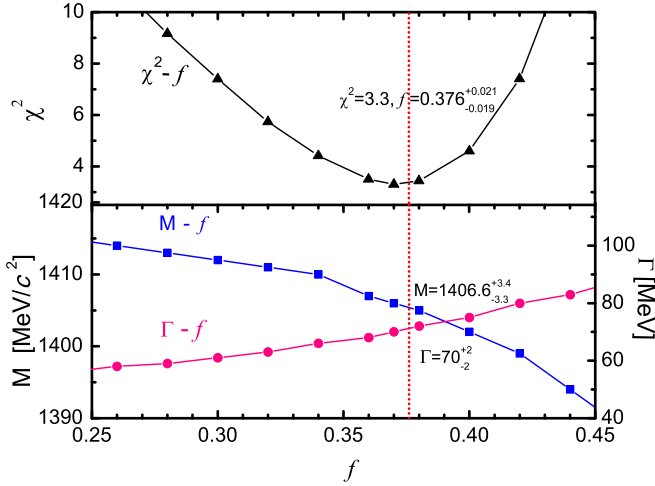


FIG. 3. (Color online) (Upper)  $\chi^2$  versus  $f$  and (lower)  $M$  and  $\Gamma$  versus  $f$ . The best fit corresponds to  $f = 0.376^{+0.021}_{-0.019}$ ,  $M = 1406.6^{+3.4}_{-3.3}$  MeV/ $c^2$ ,  $\Gamma = 70 \pm 2$  MeV, with  $\chi^2 = 3.3$  being shown by the vertical dotted line.

Changing in  $f$  alters the contribution of different channels, and the shape of the spectra is modified, where a shift of the peak position occurs. Once more, the best-fit process was iterated by varying  $f$  smoothly. In fact, we were in a four-dimensional presentation of the  $M - \Gamma - f - \chi^2$  parameters, where the minimum  $\chi^2$  occurs only at one point; when  $f$  comes close to a number of 0.376, which is equivalent to 27% of  $T_{22}$  and 73% of  $T_{21}$  contributions, the best result was obtained.

Increasing the  $f$  values causes a change in the shape of the spectrum, and makes the fit worse. In Fig. 3 we plot  $\chi^2$  versus  $f$  (upper) and  $M$  versus  $f$  (lower). The parabolic behavior of the upper figure shows a minimum value of 3.3 for  $\chi^2$ .

Different complex numbers were checked for  $f$ , but real numbers produced a better outcome. This significant shape of the spectrum is illustrated in Fig. 4 (lower), where Hemingway's data, our theoretical curve according to the best-fit parameters, and two curves of Hyodo-Weise's  $T$ -matrix calculation for  $T_{21}$  and  $T_{22}$  channels are combined together. This figure indicates that the spectra of the "chiral-weak" theory of Hyodo-Weise [13] yield  $\chi^2 = 326$  for the  $T_{21}$  channel and  $\chi^2 = 80$  for the  $T_{22}$  channel, neither of which is in agreement with the experimental data. To make better sense of these results, the confidence level (CL) contours of  $M$  versus  $\Gamma$  are depicted at three levels of confidence (68%, 95%, and 99.9%) in Fig. 4 (upper). The most probable values, which correspond to the  $1\sigma$  uncertainty, are

$$f = 0.376^{+0.021}_{-0.019}, \quad (16)$$

$$M = 1406.6^{+3.4}_{-3.3} \text{ MeV}/c^2, \quad (17)$$

$$\Gamma = 70 \pm 2 \text{ MeV} \quad (18)$$

with  $\chi^2_{\text{MIN}} = 3.3$ .

The PDG 2014 values of  $M$  and  $\Gamma$  with their error bars are also shown in the figure.

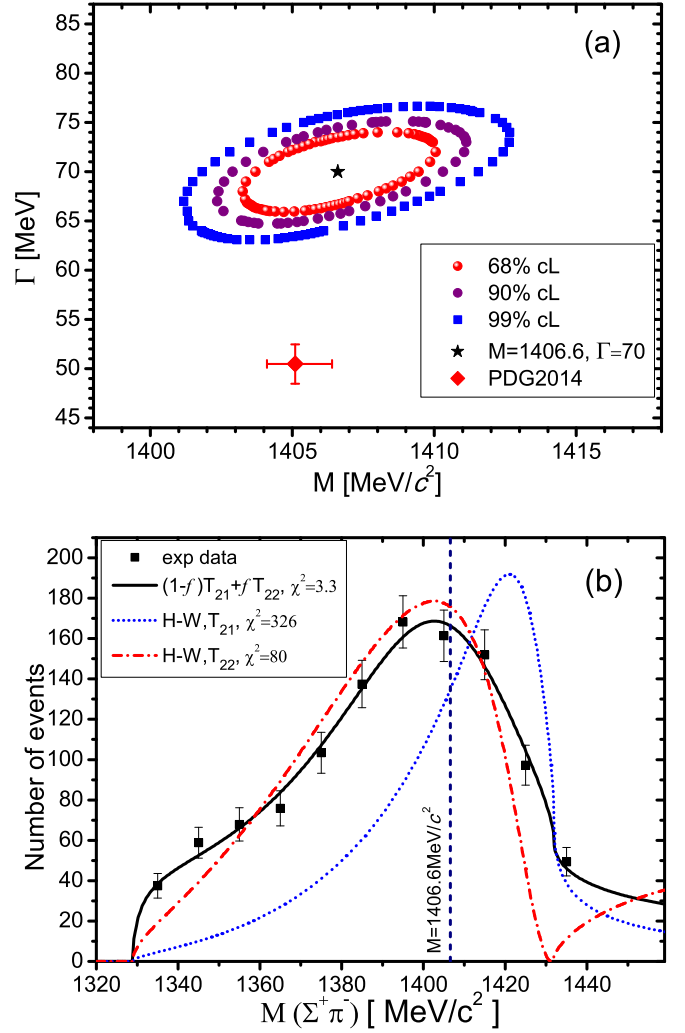


FIG. 4. (Color online) (Upper) Likelihood contour mapping of  $M_{\Sigma\pi}$  vs  $\Gamma$ , where the best-fit values are obtained in a three-dimensional fitting of the Hemingway data with  $(M, \Gamma, f)$ . The results are:  $M = 1406.6^{+3.4}_{-3.3}$  MeV/ $c^2$ ,  $\Gamma = 70 \pm 2$  MeV,  $f = 0.376^{+0.021}_{-0.019}$ , and  $\chi^2 = 3.3$ . The contour curves are given for typical values of likelihood of 68, 95, and 99.9 percent. (Lower) (solid curve) The best-fit  $M$  spectrum in our mixed  $T_{21}$  and  $T_{22}$  channel procedure. The present result is compared with individual  $|T_{21}|^2 k$  and  $|T_{22}|^2 k$  curves of Hyodo and Weise [13]. The obtained mass from the present work is shown by the vertical dashed line.

#### IV. CONCLUDING REMARKS

The invariant-mass spectra of the  $\Lambda(1405) \rightarrow \Sigma\pi$  process in the decay of  $\Sigma^+(1660)$  produced in the  $K^- + p$  reaction at 4.2 GeV were theoretically calculated and compared to experimental data of Hemingway, which covers a range from the  $\Sigma + \pi$  threshold (1330 MeV/ $c^2$ ) to the  $K^- + p$  threshold (1430 MeV/ $c^2$ ). Each spectrum shows a broad and skewed peak, reflecting both the  $\Lambda^*$  pole and the lower and upper thresholds. The two different  $T_{\Sigma\pi \leftarrow \bar{K}N}$  ( $T_{21}$ ) and  $T_{\Sigma\pi \leftarrow \Sigma\pi}$  ( $T_{22}$ ) channels were taken into account, but neither of them showed good fits to the experimental spectrum. Then, a combination of the two channels was attempted, and significantly better fits were obtained with a  $\chi^2$  minimum of 3.3. Finally, we obtained the best-fit values presented in Eqs. (16)–(18).

This result shows that the  $M$  value obtained from the Hemingway data is in good agreement with those from other old experimental data, summarized in Particle Data Group 2014, which further justifies the  $\Lambda^*$  ansatz for deeply bound  $\bar{K}$  nuclei, based on the strongly attractive  $\bar{K}N$  interaction [6–10].

## ACKNOWLEDGMENTS

This work is supported by a Grant-in-Aid for Scientific Research of Monbu-Kagakusho of Japan. One of us (M.H.) wishes to thank A. Hassasfar for discussions during this work.

- 
- [1] R. H. Dalitz and S. F. Tuan, *Ann. Phys. (NY)* **8**, 100 (1959).
  - [2] M. H. Alston *et al.*, *Phys. Rev. Lett.* **6**, 698 (1961).
  - [3] J. Beringer *et al.* (Particle Data Group), *Phys. Rev. D* **86**, 010001 (2012).
  - [4] R. H. Dalitz and A. Deloff, *J. Phys. G: Nucl. Part. Phys.* **17**, 289 (1991).
  - [5] R. J. Hemingway, *Nucl. Phys. B* **253**, 742 (1985).
  - [6] Y. Akaishi and T. Yamazaki, *Phys. Rev. C* **65**, 044005 (2002).
  - [7] T. Yamazaki and Y. Akaishi, *Phys. Lett. B* **535**, 70 (2002).
  - [8] T. Yamazaki, A. Doté, and Y. Akaishi, *Phys. Lett. B* **587**, 167 (2004).
  - [9] A. Doté, H. Horiuchi, Y. Akaishi, and T. Yamazaki, *Phys. Lett. B* **590**, 51 (2004).
  - [10] A. Doté, H. Horiuchi, Y. Akaishi, and T. Yamazaki, *Phys. Rev. C* **70**, 044313 (2004).
  - [11] T. Yamazaki and Y. Akaishi, *Phys. Rev. C* **76**, 045201 (2007).
  - [12] D. Jido, J. A. Oller, E. Oset, A. Ramos, and U. G. Meissner, *Nucl. Phys. A* **725**, 181 (2003).
  - [13] T. Hyodo and W. Weise, *Phys. Rev. C* **77**, 035204 (2008).
  - [14] Y. Akaishi, T. Yamazaki, M. Obu, and M. Wada, *Nucl. Phys. A* **835**, 67 (2010).
  - [15] D. B. Kaplan and A. E. Nelson, *Phys. Lett. B* **175**, 57 (1986).
  - [16] G. E. Brown, C. H. Lee, M. Rho, and V. Thorsson, *Nucl. Phys. A* **567**, 937 (1994).
  - [17] O. Braun *et al.*, *Nucl. Phys. B* **129**, 1 (1977).
  - [18] I. Zychor *et al.*, *Phys. Lett. B* **660**, 167 (2008).
  - [19] J. Esmaili, Y. Akaishi, and T. Yamazaki, *Phys. Lett. B* **686**, 23 (2010).
  - [20] J. Esmaili, Y. Akaishi, and T. Yamazaki, *Phys. Rev. C* **83**, 055207 (2011).
  - [21] B. Riley, I.-T. Wang, J. G. Fetkovich, and J. M. McKenzie, *Phys. Rev. D* **11**, 3065 (1975).
  - [22] M. Hassanvand, S. Z. Kalantari, Y. Akaishi, and T. Yamazaki, *Phys. Rev. C* **87**, 055202 (2013); **88**, 019905(E) (2015).
  - [23] G. Agakishiev *et al.* (HADES Collaboration), *Phys. Rev. C* **87**, 025201 (2013).
  - [24] K. A. Olive *et al.* (Particle Data Group), *Chin. Phys. C* **38**, 090001 (2014).
  - [25] M. Agnello *et al.*, *Phys. Rev. Lett.* **94**, 212303 (2005).
  - [26] T. Yamazaki *et al.*, *Phys. Rev. Lett.* **104**, 132502 (2010); P. Kienle *et al.*, *Eur. Phys. J. A* **48**, 183 (2012).
  - [27] Y. Ichikawa *et al.*, *Porg. Exp. Theor. Phys.* **2015**, 021D01 (2015).
  - [28] Y. Akaishi, K. S. Myint, and T. Yamazaki, *Proc. Jpn. Acad. B* **84**, 264 (2008).
  - [29] L. S. Geng and E. Oset, *Eur. Phys. J. A* **34**, 405 (2007).
  - [30] H. Feshbach, *Ann. Phys. (NY)* **5**, 357 (1958); **19**, 287 (1962).
  - [31] M. Hassanvand *et al.*, arXiv:1510.00870.